J Supercond Nov Magn (2013) 26:429–435
DOI 10.1007/s10948-012-1758-z

ORIGINAL PAPER

Catalytic Activity of the Spinel Ferrite Nanocrystals on the Growth of Carbon Nanotubes

R. Hosseini Akbarnejad · V. Daadmehr · A.T. Rezakhani · F. Shahbaz Tehrani · F. Aghakhani · S. Gholipour

Received: 26 June 2012 / Accepted: 17 August 2012 / Published online: 9 September 2012

Abstract We prepared three ferrite nanocatalysts: (i) copper ferrite ($CuFe_2O_4$) (ii) ferrite where cobalt was substituted by nickel ($Ni_xCo_{1-x}Fe_2O_4$, with $x = 0$, 0.2, 0.4, 0.6), and (iii) ferrite where nickel was substituted by zinc ($Zn_yNi_{1-y}Fe_2O_4$ with $y = 1$, 0.7, 0.5, 0.3), by the sol-gel method. The X-ray diffraction patterns show that the ferrite samples have been crystallized in the cubic spinel structural phase. We obtained the size of grains by field emission scanning electron microscopy images and their magnetic properties by vibrating sample magnetometer. Next, carbon nanotubes were grown on these nanocatalysts by the catalytic chemical vapor deposition method. We show that the catalytic activity of these nanocrystals on the carbon nanotube growth depend on cation distributions in the octahedral and tetrahedral sites, structural isotropy, and catalytic activity due to cations. Our study may have applications in finding a suitable candidate of doped ferrite nanocrystals as catalysts for carbon nanotube growth. More interestingly, the yield of fabrication of carbon nanotubes can be considered as an indirect tool to study catalytic activity of ferrites.

Keywords Carbon nanotubes 61.48.De · Catalysis 81.16.Hc · Chemical vapor deposition 81.15.Gh · Crystal structure 61.05.c- · Ferrites 75.50.Gg · Sol-gel processing 81.20.Fw

R. Hosseini Akbarnejad · V. Daadmehr (✉) · F. Shahbaz Tehrani · F. Aghakhani · S. Gholipour
Magnet and Superconducting Research Lab., Department of Physics, Alzahra University, Tehran 19938, Iran
e-mail: daadmehr@alzahra.ac.ir
url: http://www.alzaha.ac.ir/daadmehr/

R. Hosseini Akbarnejad
e-mail: rh.akbarnejad@gmail.com

F. Shahbaz Tehrani
e-mail: tehrani66@gmail.com

F. Aghakhani
e-mail: faezeh.aghakhani@yahoo.com

S. Gholipour
e-mail: gholipour66@gmail.com

A.T. Rezakhani
Department of Physics, Sharif University of Technology, Tehran, Iran
e-mail: rezakhani@sharif.edu

1 Introduction

In the spinel ferrites of MFe_2O_4, the metallic cations M^{2+} and Fe^{3+} can occupy octahedral and tetrahedral sites. If the M^{2+} cations occupy tetrahedral sublattices in the cubic closed-packed O^{2-} lattice, the spinel ferrite is a normal spinel; otherwise, the ferrite is an inverse spinel. If both of the sublattices contain M^{2+} and Fe^{3+} cations, the ferrite is a mixed spinel. The occupations of cations at these sites have a significant effect on the properties of spinels, such as magnetic behavior, conductivity, and catalytic activity [1–3]. Mixed nickel ferrites with different magnetization and various cation distributions form an important class of magnetic materials [4].

Ni/Zn ferrites have the mixed spinel structure with the unit cell consisting of eight units of the form $[Zn_x{}^{2+}Fe_{1-x}{}^{3+}]_{tet}$ $[Ni_{1-x}{}^{2+}Fe_{1+x}{}^{3+}]_{oct}O_4{}^{2-}$. The Zn^{2+} cations preferably occupy the tetrahedral sites and the Ni^{2+} cations always occupy the octahedral sites [5]. In Ni/Co ferrites the cation distribution of Co^{2+} depends on heat treatment [6, 7]. As an application, spinel ferrites can acts as good catalysts [8]. The catalytic activity of these materials was studied in some chemical reactions such as decomposition of hydrogen peroxide [9], oxidation of carbon monoxide [10], and oxidative dehydrogenation of butane [11].

Chemical composition, crystal structure, electronic, electrochemical, and micro structural factors have been found to contribute to the overall activity of such catalysts [9]. Since the nano-sized catalysts with non-zero magnetic moment are widely used for growth of carbon nanotubes (CNTs), it is of paramount practical and theoretical importance to investigate the catalytic activity of spinel ferrite nanocrystals on the growth of CNTs.

In this paper, we study the catalytic effect of Ni/Co ferrites ($Ni_xCo_{1-x}Fe_2O_4$ with $x = 0, 0.2, 0.4, 0.6$), Ni/Zn ferrites ($Zn_yNi_{1-y}Fe_2O_4$ with $y = 0.3, 0.5, 0.7, 1$), and copper ferrite ($CuFe_2O_4$) on the growth of CNTs by the catalytic chemical vapor deposition (CCVD) method. Specifically, we investigate the occupation effect of ferromagnetic ions Fe^{3+}, Co^{2+}, Ni^{2+} and non-magnetic ions such as Cu^{2+} and Zn^{2+} in the tetrahedral and octahedral sites of ferrospinels on their catalytic activity for growth of CNTs.

2 Experiment

2.1 Preparation of Catalyst

The sol-gel method is one of the best procedures for fabricating the ferrite nanocrystals. Thus in our experiment, Ni/Co, Ni/Zn, and Cu ferrites were all prepared by this method. In this way, with the stoichiometric laws, (depending on the combination), we prepared 0.5 M solutions of $Fe(NO_3)_3{\cdot}9H_2O$ (98 %), $Co(NO_3)_2{\cdot}6H_2O$ (98 %), $Ni(NO_3)_2{\cdot}6H_2O$ (99 %), $Zn(NO_3)_2{\cdot}3H_2O$ (99 %) and $Cu(NO_3)_2{\cdot}3H_2O$ (99 %); and added these solutions to 0.5 M solution of citric acid with 1:1 mol ratio for nitrates:citric acid. The pH value of the solution was adjusted to 1 by ethylenediamine in order to make the environment more conducive for generating fine particles. The prepared solution was baked in 70 °C to form a brown gel. The obtained gel was dried in 135 °C during 24 hours and was ground into a fine powder. Finally, the sample was calcined in 450–600 °C range (depending on the doping value of the ferrites) for 4 hours.

2.2 Growth of Carbon Nanotubes

The CNTs were grown by the CCVD method in a quartz reactor with a programmable furnace. The carbon source was acetylene (C_2H_2) with argon (Ar) as the carrier gas. To synthesize, an alumina boat containing 0.05 g of catalyst was placed in the hot zone of the quartz reactor. A mixture of C_2H_2 and Ar with 1:8 volume ratios was passed over the catalyst in atmospheric pressure. The temperature was risen with the rate of 5 °C/min. to a specific temperature that depending on the crystallization temperature of each catalyst, and the reaction time was 45 minutes. Since the cation distribution of ferrites depends on heat treatment [6, 7], the growth temperatures were selected equal to the calcination temperatures. The amount of carbon was evaluated by the mass of the fabricated samples. These samples contain amorphous carbons, CNTs, and catalyst. In order to remove the amorphous carbons, we oxidized the samples in the air at 400 °C for 1 hour.

2.3 Characterization

X-ray diffraction (XRD) patterns of the synthesized nanocatalysts were obtained using a Philips® PW1800 X-ray diffractometer with Cu Kα radiation ($\lambda = 1.54056$ Å) operated at 40 kV and 30 mA. The refinement method of Rietveld was applied with the "Material Analysis Using Diffraction" (MAUD) program (v.2.056) for the XRD patterns of nanocatalysts. The average grain size and morphology of the nanocatalysts were observed by a Hitachi® S4160 Field Emission Scanning Electron Microscopy (FE-SEM). The magnetic properties of the samples were measured by Meghnatis Daghigh Kavir Co.® Vibrating Sample Magnetometer (VSM) at the room temperature. The maximum applied field during such measurements was 9 kOe. Also, we characterized the CNTs by these X-ray diffractometer and FE-SEM.

3 Results and Discussion

3.1 Structural Studies of Nanocatalysts

We studied the crystalline structure of the ferrite nanocatalysts with the XRD analysis. Figure 1 shows the XRD pattern of the prepared nanocrystals. These patterns were compared with the Joint Committee on Powder Diffraction Standards (JCPDS). The presence of (220), (311), (400), (422), (511), and (440) major lattice planes revealed the cubic spinel phase with Fd3m space group. In addition, the minor lattice planes of (111) and (222) are present. These results emphasize the presence of only spinel phase without any significant impurities. The XRD pattern of samples was refined by using the MAUD software and Reitveld method for structural analysis, cation distribution, and lattice parameter calculation. Crystallographic properties of the samples were obtained from this calculation and are listed in Table 1. We report the details of the MAUD analysis for Ni/Zn and Cu ferrite nanocatalysts in the other paper. Table 2 shows the before- and after-refinement values indicating high accuracy in synthesizing the nanocatalysts without formation of extra phases. The pattern fitness can be checked for XRD data. There are several parameters for the calculation of pattern fitness. The goodness of fit (S) is described by $S = R_{wp}/R_{exp}$, where R_{wp} is the weighted residual error

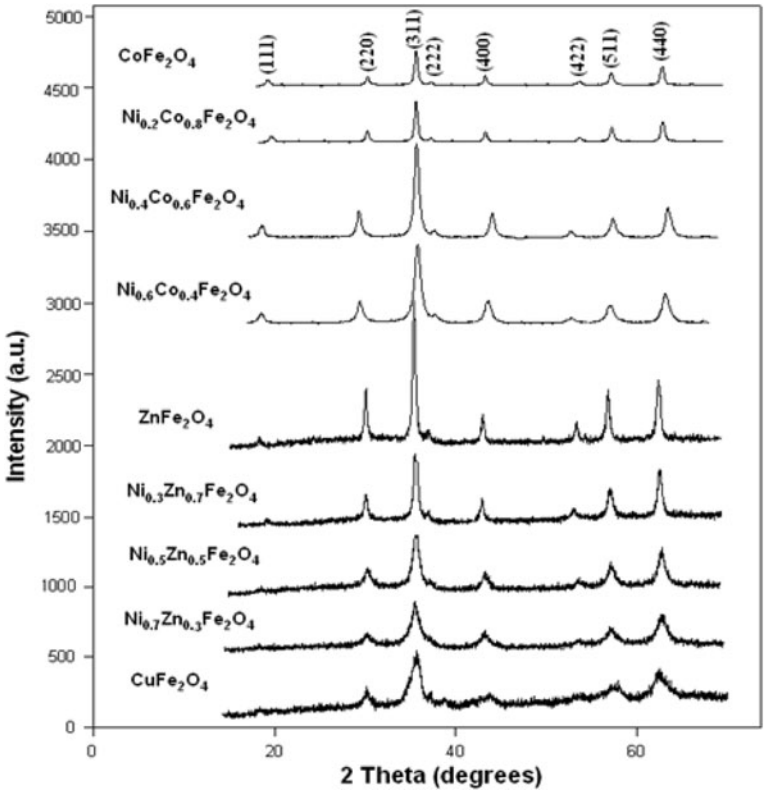

Fig. 1 The XRD pattern of the ferrite nanocatalysts

Table 1 Magnetic and crystallographic properties of ferrite nanocatalysts

Ferrite	Cation distribution	Degree of inversion	a (Å)	M_S (emu/g)	H_c (Oe)
$CoFe_2O_4$	$[Fe^{3+}]_{tet}$ $[Co^{2+}, Fe^{3+}]_{oct}$	1	8.390	69.9	1186
$Ni_{0.2}Co_{0.8}Fe_2O_4$	$[Fe^{3+}]_{tet}$ $[Ni^{2+}{}_{0.2}, Co^{2+}{}_{0.8}, Fe^{3+}]_{oct}$	1	8.377	58.1	1013
$Ni_{0.4}Co_{0.6}Fe_2O_4$	$[Fe^{3+}]_{tet}$ $[Ni^{2+}{}_{0.4}, Co^{2+}{}_{0.6}, Fe^{3+}]_{oct}$	1	8.356	47.9	877
$Ni_{0.6}Co_{0.4}Fe_2O_4$	$[Fe^{3+}]_{tet}$ $[Ni^{2+}{}_{0.6}, Co^{2+}{}_{0.4}, Fe^{3+}]_{oct}$	1	8.356	27.1	400
$ZnFe_2O_4$	$[Zn^{2+}]_{tet}$ $[Fe^{3+}, Fe^{3+}]_{oct}$	0	8.430	1.6	3.3
$Ni_{0.3}Zn_{0.7}Fe_2O_4$	$[Zn^{2+}{}_{0.7}, Fe^{3+}{}_{0.3}]_{tet}$ $[Ni^{2+}{}_{0.3}, Fe^{3+}{}_{1.7}]_{oct}$	0.3	8.400	28.4	0.3
$Ni_{0.5}Zn_{0.5}Fe_2O_4$	$[Zn^{2+}{}_{0.5}, Fe^{3+}{}_{0.5}]_{tet}$ $[Ni^{2+}{}_{0.5}, Fe^{3+}{}_{1.5}]_{oct}$	0.5	8.390	34.8	0.1
$Ni_{0.7}Zn_{0.3}Fe_2O_4$	$[Zn^{2+}{}_{0.3}, Fe^{3+}{}_{0.7}]_{tet}$ $[Ni^{2+}{}_{0.7}, Fe^{3+}{}_{1.3}]_{oct}$	0.7	8.370	25.7	0.1
$CuFe_2O_4$	$[Fe^{3+}]_{tet}[Cu^{2+}, Fe^{3+}]_{oct}$	1	8.372	14.8	168.1

and R_{exp} is the expected error. Refinement has been continued until a convergence was reached for a value of S close to 1 which confirms the goodness of refinement. These parameters are listed in Table 3. This study indicates the inverse spinel structure for Ni/Co and copper ferrites. This means that in the Ni/Co ferrites, the Ni^{2+} and Co^{2+} cations occupy the octahedral sites, and the Fe^{3+} cations occupy the octahedral and tetrahedral sites equally; and, in the copper ferrite the Cu^{2+} cations fill only the half of the octahedral sites. This study shows as well the normal spinel structure for the zinc ferrite and mixed spinel structure for the Ni/Zn ferrites because the Ni^{2+} cations occupy the octahedral and the Zn^{2+} cations occupy the tetrahedral sites. Notice that these results are consistent with Ref. [5].

The lattice constant of the samples were obtained from the formula $a = d\ (h^2 + k^2 + l^2)^{1/2}$, where d is the interplane spacing and is calculated from the position of the highest peak in the XRD pattern (here (311) plane) by Bragg's formula (and refined later by using MAUD software). In Table 1, we observe that the lattice constant increases with the Co content in the Ni/Co ferrites and the Zn content in the Ni/Zn ferrites. This can be attributed to the higher ionic radii of Co^{2+} (0.79 Å) and Zn^{2+} (0.82 Å) compared to Ni^{2+} (0.69 Å).

3.2 Magnetic Study of Nanocatalysts

The magnetic properties of the nanocrystals were measured by VSM at the room temperature (∼25 °C). The coercivity

Table 2 Structural parameters before and after refinement from MAUD analysis for $Ni_xCo_{1-x}Fe_2O_4$ nanocrystals

Composition	Structural parameters before refinement						Structural parameters after refinement					
	Ions	Position			Occupancy	Quantity	Ions	Position			Occupancy	Quantity
		X (Å)	Y (Å)	Z (Å)				X (Å)	Y (Å)	Z (Å)		
$Ni_{0.6}Co_{0.4}Fe_2O_4$	$Fe^{3+}{}_{(tet)}$	0	0	0	1	8	$Fe^{3+}{}_{(tet)}$	$-2.7 \times 10^{-7} \approx 0$	$-1.0 \times 10^{-6} \approx 0$	$-9.2 \times 10^{-7} \approx 0$	1.00005	8.00038
	$Fe^{3+}{}_{(oct)}$	0.625	0.625	0.625	0.5	8	$Fe^{3+}{}_{(oct)}$	0.625074	0.625712	0.6245	0.49999	7.99997
	$Co^{2+}{}_{(oct)}$	0.625	0.625	0.625	0.2	3.2	$Co^{2+}{}_{(oct)}$	0.624698	0.625298	0.624804	0.199998	3.19997
	$Ni^{2+}{}_{(oct)}$	0.625	0.625	0.625	0.3	4.8	$Ni^{2+}{}_{(oct)}$	0.624798	0.625197	0.624714	0.299999	4.79998
	O^{2-}	0.3825	0.3825	0.3825	1	32	O^{2-}	0.382499	0.3825001	0.3825012	1.000003	32.0001
$Ni_{0.4}Co_{0.6}Fe_2O_4$	$Fe^{3+}{}_{(tet)}$	0	0	0	1	8	$Fe^{3+}{}_{(tet)}$	$1.6 \times 10^{-8} \approx 0$	$-2.9 \times 10^{-9} \approx 0$	$3.9 \times 10^{-9} \approx 0$	1.00130	8.01043
	$Fe^{3+}{}_{oct}$	625	0.625	0.625	0.5	8	$Fe^{3+}{}_{(oct)}$	0.625456	0.625458	0.625460	0.49912	7.99859
	$Co^{2+}{}_{(oct)}$	0.625	0.625	0.625	0.3	4.8	$Co^{2+}{}_{(oct)}$	0.625446	0.625468	0.625477	0.29994	4.79899
	$Ni^{2+}{}_{(oct)}$	0.625	0.625	0.625	0.2	3.2	$Ni^{2+}{}_{(oct)}$	0.625454	0.625499	0.625469	0.19989	3.19837
	O^{2-}	0.3825	0.3825	0.3825	1	32	O^{2-}	0.3818384	0.382035	0.382838	0.98648	31.9768
$Ni_{0.2}Co_{0.8}Fe_2O_4$	$Fe^{3+}{}_{(tet)}$	0	0	0	1	8	$Fe^{3+}{}_{(tet)}$	$-2.3 \times 10^{-9} \approx 0$	$-1.3 \times 10^{-7} \approx 0$	$-8.7 \times 10^{-9} \approx 0$	1.00009	8.00073
	$Fe^{3+}{}_{(oct)}$	0.625	0.625	0.625	0.5	8	$Fe^{3+}{}_{(oct)}$	0.625476	0.625442	0.625467	0.50038	8.00623
	$Co^{2+}{}_{(oct)}$	0.625	0.625	0.625	0.4	6.4	$Co^{2+}{}_{(oct)}$	0.625448	0.625460	0.625449	0.40036	6.40574
	$Ni^{2+}{}_{(oct)}$	0.625	0.625	0.625	0.1	1.6	$Ni^{2+}{}_{(oct)}$	0.625471	0.625463	0.625456	0.10033	1.60533
	O^{2-}	0.3825	0.3825	0.3825	1	32	O^{2-}	0.382482	0.381655	0.383165	0.99999	31.9998
$CoFe_2O_4$	$Fe^{3+}{}_{(tet)}$	0	0	0	1	8	$Fe^{3+}{}_{(tet)}$	$1.2 \times 10^{-7} \approx 0$	$8.5 \times 10^{-8} \approx 0$	$2.9 \times 10^{-7} \approx 0$	0.999937	7.99949
	$Fe^{3+}{}_{(oct)}$	0.625	0.625	0.625	0.5	8	$Fe^{3+}{}_{(oct)}$	0.6245	0.625265	0.625437	0.500048	8.00077
	$Co^{2+}{}_{(oct)}$	0.625	0.625	0.625	0.5	8	$Co^{2+}{}_{(oct)}$	0.625044	0.624634	0.625304	0.500044	8.00071
	O^{2-}	0.3825	0.3825	0.3825	0.3825	32	O^{2-}	0.379984	0.379881	0.379959	1.000036	32.0012

(H_c) and the saturation magnetization (M_S) of the nanocatalysts are listed in Table 1. H_c of Ni/Co ferrites decrease inversely with the nickel content since the coercivity of a magnetic material is a measure of magneto-crystalline anisotropy. This decrease is attributed to the lower magneto-crystalline anisotropy of nickel as compared to cobalt, which in turn leads to a lower coercivity. According to the MAUD analysis, the Ni/Co and Cu ferrites are inverse spinels. The decrease in M_S of Ni/Co ferrites with the increase of Ni content is attributed to the smaller magnetic moment of the Ni^{2+} ($2\mu_B$) as compared to the Co^{2+} ($3\mu_B$). In addition, the M_S of $CoFe_2O_4$ is more than $CuFe_2O_4$ as a result of the higher magnetic moment of Co^{2+} ($3\mu_B$) than Cu^{2+} ($1\mu_B$). As we explain in our other work, the Ni/Zn ferrites as a result of near zero H_c show superparamagnetic behavior at room temperature. The cation distribution of the zinc ferrite, zero magnetic moment of the Zn^{2+} cations, and the anti-ferromagnetic interactions between the Fe^{3+} cations in the octahedral sites cause the magnetic moment (M_S) for each $ZnFe_2O_4$ formula to vanish. The cation distribution changes by the substitution of Zn^{2+} by Ni^{2+} cations and occupation of the octahedral sites with Ni^{2+} cations; thus this substitution transfer part of the Fe^{3+} cations to the tetrahedral sites, and accordingly makes the M_S of the nanocrystals vary. This is consistent with Néel's ferrimagnetic theory [12]. This behavior of the Ni/Zn ferrite nanocrystals for the different values of M_S is similar to that of bulk samples [5]. It is important to notice that the maximum M_S is found in the $Zn_{0.5}Ni_{0.5}Fe_2O_4$ nanocrystals.

Table 3 The parameters for the calculational pattern fitness for $Ni_xCo_{1-x}Fe_2O_4$ nanocrystals

X	R_w	R_b	R_{exp}	S
0	0.373	0. 309	0.311	1.20
0.2	0.315	0.254	0.299	1.05
0.4	0.153	0. 130	0.142	1.07
0.6	0.152	0.129	0.142	1.06

3.3 Morphological Study of Nanocatalysts

The FE-SEM images of the nanocatalysts are shown in Fig. 2. We observe that the prepared nanocrystals have a spherical morphology and cohesion of particles is due to the magnetic attraction. The average grains diameters of the nanocrystals (D_{ave}) were obtained from the FE-SEM images and are listed in Table 3. In addition, the surfaces/gram ratios of the nanocatalysts (S) were found from dividing the average surface of a particle by its mass.

3.4 XRD and FE-SEM Studies of Carbon Nanotubes

The samples were characterized by XRD after the growth of CNTs. Figure 3 shows these XRD patterns. The (002), (100), (101), (004) and (110) peaks are related to the presence of the CNTs. The presence of the (002) plane between $2\theta = 26$–$26.5°$ is due to the presence of multiwall CNTs (MWNTs) [13]. According to Ref. [14], the (110) and (100)

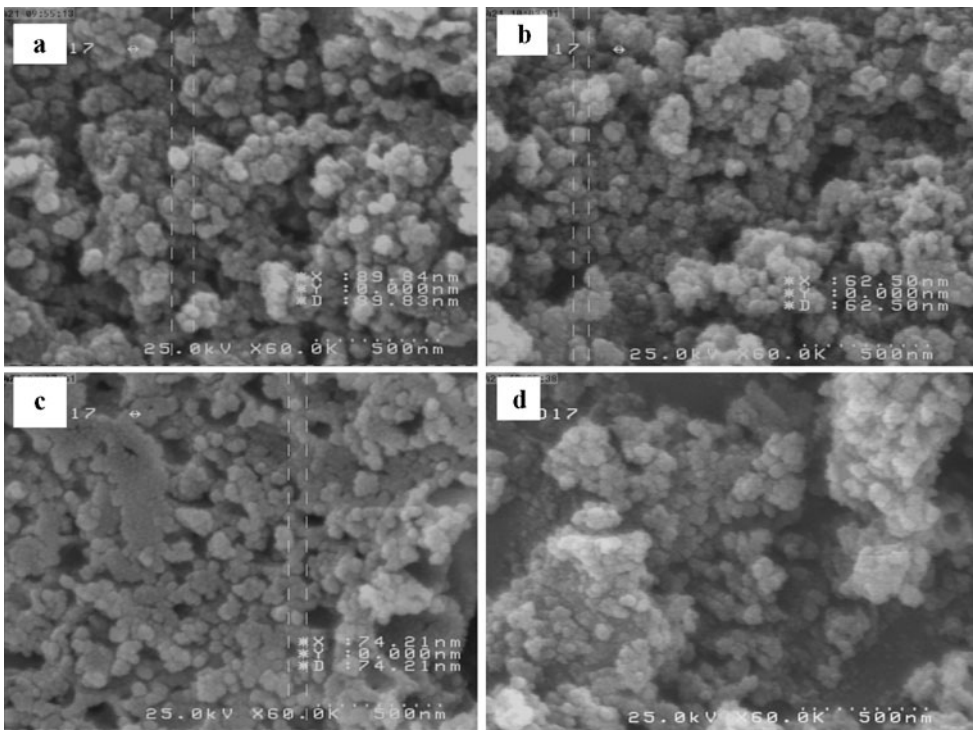

Fig. 2 The FE-SEM images from the nanocatalysts (**a**) $Ni_{0.4}Co_{0.6}Fe_2O_4$, (**b**) $CuFe_2O_4$, (**c**) $ZnFe_2O_4$, (**d**) $CoFe_2O_4$

peaks are in the (hk0) group peaks and display an asymmetric shape due to the curvature of the CNT. The (004) and (101) reflections are also due to flat graphitic layers, residual carbon particles, and the defect of the CNTs [15, 16].

Figure 4 is shows the FE-SEM images of the CNTs obtained on these nanocatalysts. The particles of the nanocatalysts are observed in the top of the CNTs. The CNTs are not uniformly straight because of catalyst particle movements during the growth process [17]. These movements induce structural defects that were observed in the XRD patterns by the (101) and (004) peaks.

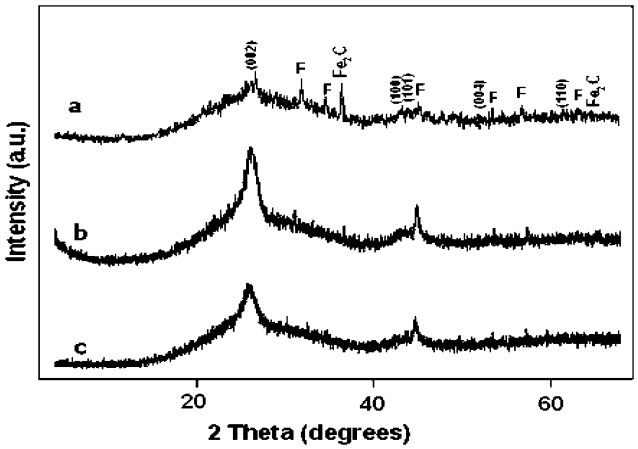

Fig. 3 XRD patterns of the CNTs obtained on (**a**) $ZnFe_2O_4$, (**b**) $CoFe_2O_4$, and (**c**) $CuFe_2O_4$ (F: peaks are related to the ferrites)

3.5 Catalytic Activity of Nanocatalysts

The catalytic activity of the spinel ferrite nanocatalysts for the growth of the CNTs is evaluated by the rate of production of the CNTs in the surface unit of all nanocatalysts. This parameter was obtained by normalizing the amount of the CNTs to unit time, surface, and mass of the catalysts in the crystallization temperature of each catalyst.

In Table 4, we observe that the catalytic activity of the Ni/Co ferrites increases with the nickel content—as a result of higher catalytic activity of Ni in comparison to Co. Besides, in the Ni/Zn ferrites it is observed that $Ni_{0.5}Zn_{0.5}Fe_2O_4$ has the highest catalytic activity while $ZnFe_2O_4$ comes next. The grown CNTs on $ZnFe_2O_4$ are

Table 4 Dimensions and catalytic activity of ferrite nanocatalysts

Ferrite	D_{ave} (nm)	S (m^2/g)	Catalytic activity ($m^{-2}\,min^{-1}$) $\times 10^{-3}$
$CoFe_2O_4$	71.9	15.8	2.8
$Ni_{0.2}Co_{0.8}Fe_2O_4$	53.8	21.1	7.3
$Ni_{0.4}Co_{0.6}Fe_2O_4$	56.5	19.9	8.7
$Ni_{0.6}Co_{0.4}Fe_2O_4$	57.1	19.7	10.4
$ZnFe_2O_4$	34.6	16.2	1.7
$Ni_{0.3}Zn_{0.7}Fe_2O_4$	42.5	13.2	1.2
$Ni_{0.5}Zn_{0.5}Fe_2O_4$	25.8	21.7	2.2
$Ni_{0.7}Zn_{0.3}Fe_2O_4$	24.6	22.8	1.3
$CuFe_2O_4$	37.62	14.7	2.6

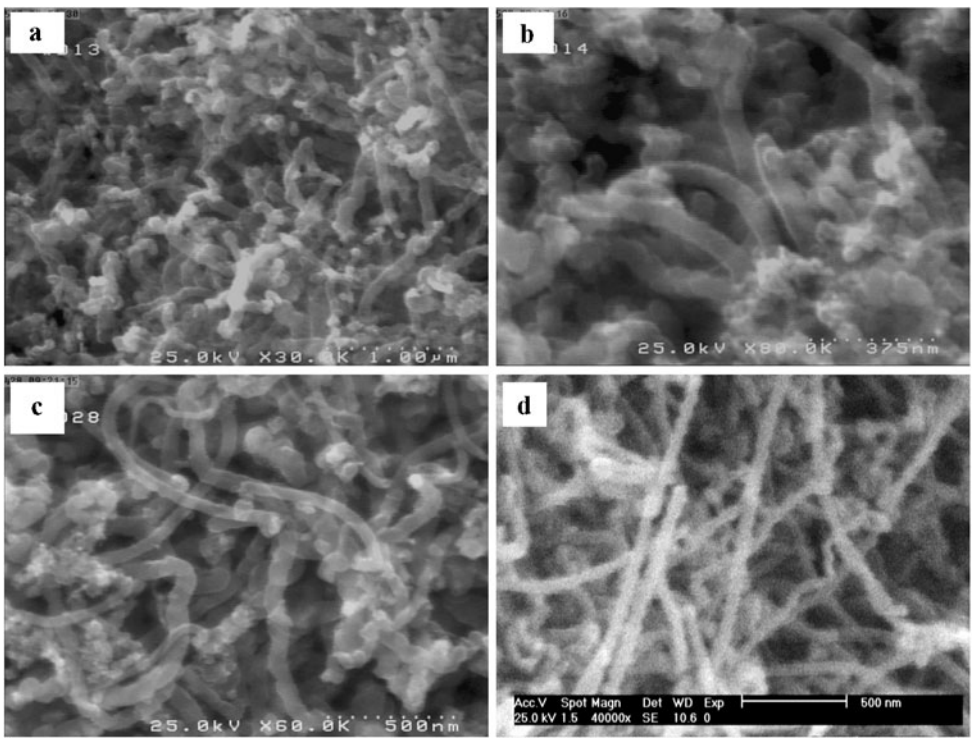

Fig. 4 FE-SEM images from grown CNTs on (**a**) $Ni_{0.4}Co_{0.6}Fe_2O_4$, (**b**) $CuFe_2O_4$, (**c**) $ZnFe_2O_4$, (**d**) $CoFe_2O_4$

more pure than CNTs grown on $Zn_{0.5}Ni_{0.5}Fe_2O_4$. As mentioned above, in the $ZnFe_2O_4$ nanocatalyst, Zn^{2+} cations occupy the tetrahedral sites and all of these sites are in the same conditions. Thus the octahedral sites are isotropic. This structural isotropy enhances the catalytic activity. With the decrease in the Zn^{2+} content and entrance of the Ni^{2+} cations into the structure, the Ni^{2+} cations occupy the octahedral sites and transfer part of Fe^{3+} to the tetrahedral sites. These changes cause a decrease in the structural isotropy and the catalytic activity of $Ni_{0.3}Zn_{0.7}Fe_2O_4$ and $Ni_{0.7}Zn_{0.3}Fe_2O_4$ nanocatalysts. Because of the occupation of the half of tetrahedral sites with Zn^{2+} and remainder with Fe^{3+}, the $Ni_{0.5}Zn_{0.5}Fe_2O_4$ nanocatalyst has a structural isotropy, and thus the catalytic activity increases. This isotropy exists completely in the tetrahedral sites of the inverse spinels. This fact makes the catalytic activity of the copper ferrite nanocrystals increase compared to zinc ferrite—see Ref. [11], where the oxidative dehydrogenation of butenes in the presence of ferrospinel catalysts have been considered. Moreover, the catalytic activity of the Ni/Co ferrites is more than the copper ferrite because the catalytic activity due to Ni^{2+} and Co^{2+} in the growth of CNTs is high in comparison to Cu^{2+}. Besides, it notices that the catalytic activity and the magnetic properties (M_S, and H_c) of the nanocatalysts are not in the same manner—see Tables 1 and 3. The studies in this issue are continued.

4 Conclusion

In summary, we prepared Ni/Co, Ni/Zn, and Cu ferrites by the sol-gel method. XRD showed the cubic spinel structure for all of these ferrites. The MAUD analysis on the XRD patterns confirmed the inverse spinel structure for the Ni/Co and Cu ferrites, the normal spinel for Zn ferrite, and the mixed spinel for the Ni/Zn ferrites. Magnetic properties of these nanocrystals were measured by VSM at the room temperature. M_S and H_c of the Ni/Co ferrites were shown to decrease with the increase of the nickel content because the magnetic moment of Ni^{2+} as compared to Co^{2+} and magneto-crystalline anisotropy of Ni as compared to Co are lower. The behavior of the Ni/Zn ferrite nanocrystals with different values of M_S appeared similar to that in bulk samples. The maximum M_S was found in the $Zn_{0.5}Ni_{0.5}Fe_2O_4$ nanocrystals. The catalytic activities of these nanocatalysts were obtained from the growth of the CNTs on them. We found that the catalytic activity of the spinel ferrites is related to the structural isotropy, the cation distribution, and the catalytic activity of cations. Hence, the catalytic activity of the Ni/Co ferrites increases with the increase in the Ni content due to higher catalytic activity of Ni compared to Co. In the Ni/Zn ferrites, the structural isotropy is an effective factor for their catalytic activity. The catalytic activity of Cu ferrite is higher than the Ni/Zn ferrites since it is inverse spinel, and less than Ni/Co ferrites as a result of the catalytic activity due to cations.

Briefly, we have found that the catalytic activity has the following order: $Ni_{0.6}Co_{0.4}Fe_2O_4 > Ni_{0.4}Co_{0.6}Fe_2O_4 > Ni_{0.2}Co_{0.8}Fe_2O_4 > CoFe_2O_4 > CuFe_2O_4 > Zn_{0.5}Ni_{0.5}Fe_2O_4 > ZnFe_2O_4 > Ni_{0.7}Zn_{0.3}Fe_2O_4 > Ni_{0.3}Zn_{0.7}Fe_2O_4$.

Acknowledgements The authors acknowledge the Iranian Nano Technology Initiative Council and Vice Chair for research of Alzahra University.

References

1. Bersuker, I.B.: Electronic Structure and Properties of Transition Metal Compounds: Introduction to the Theory. Wiley, New York (1996)
2. Burns, R.: Mineralogical Applications of Crystal Field Theory, vol. 5. Cambridge University Press, Cambridge (1993)
3. Borg, R.J., Dienes, G.J.: Physical Chemistry of Solids. Academic Press, San Diego (1992)
4. El-Sayed, A.M.: Electrical conductivity of nickel–zinc and Cr substituted nickel–zinc ferrites. Mater. Chem. Phys. **82**, 583 (2003)
5. Goldman, A.: Modem Ferrite Technology, 2nd edn., pp. 63–71. Springer, Pittsburgh (1987). ISBN 10: 0-387-29413-9
6. Ferreira, T.A.S., Waerenborgh, J.C., Mendonca, M.H.R.M., Nunes, M.R., Costa, F.M.: Structural and morphological characterization of $FeCo_2O_4$ and $CoFe_2O_4$ spinels prepared by a coprecipitation method. Solid State Sci. **5**, 383 (2003)
7. Murray, P.J., Linnette, J.W.: Cation distribution in the spinels $Co_xFe_{3-x}O_4$. J. Phys. Chem. Solids **37**, 1041 (1976)
8. Lahiri, P., Sengupta, S.K.: Spinel ferrites as catalyst: a study on catalytic effect of coprecipitated ferrites on hydrogen peroxide decomposition. Can. J. Chem. **69**, 33 (1991)
9. Goldstein, J.R., Tseung, A.C.C.: The kinetics of hydrogen peroxide decomposition catalyzed by cobalt-iron oxides. J. Catal. **32**, 452 (1974)
10. Krishnamurthy, K.R., Viswanathan, B., Sastri, M.V.C.: Catalytic activity of transition metal spinel type ferrites: structure-activity correlations in the oxidation of CO. J. Res. Inst. Catal, Hokkaido Univ. **24**, 219 (1976)
11. Massoth, F.E., Scarpiello, P.A.: Catalyst characterization studies on the Zn–Cr–Fe oxide system. J. Catal. **21**, 294 (1971)
12. Néel, L.: Magnetic properties of femtes: ferrimagnetism and antiferromagnetism. Ann. Phys. Paris **3**, 137 (1948)
13. Belin, T., Epron, F.: Characterization methods of carbon nanotubes: a review. Mater. Sci. Eng. B, Solid-State Mater. Adv. Technol. **119**, 105 (2005)
14. Lambin, P., Loiseau, A., Culot, C., Biro, L.: Structure of carbon nanotubes probed by local and global probes. Carbon **40**, 1635 (2002)
15. Liu, M., Cowley, J.: Structures of the helical carbon nanotubes. Carbon **32**, 393 (1994)
16. Bernaerts, D., Amelinckx, S., Lambin, P., Lucas, A.: The diffraction space of circular and polygonized multishell nanotubules. Appl. Phys. A **67**, 53 (1998)
17. Figueiredo, J.L., Orfao, J.J.M., Cunha, A.F.: Hydrogen production via methane decomposition on Raney-type catalysts. Int. J. Hydrog. Energy **35**, 9795 (2010)